Promotion effect of nanosized Pt, RuO_2 and NiO_x loading on visible light-driven photocatalysts $K_4Ce_2M_{10}O_{30}$ (M=Ta, Nb) for hydrogen evolution from water decomposition

2007 Sci. Technol. Adv. Mater. 8 82

(http://iopscience.iop.org/1468-6996/8/1-2/A15)

Available online at www.sciencedirect.com
ScienceDirect
Science and Technology of Advanced Materials 8 (2007) 82–88
SCIENCE AND TECHNOLOGY OF ADVANCED MATERIALS
www.elsevier.com/locate/stam

Promotion effect of nanosized Pt, RuO_2 and NiO_x loading on visible light-driven photocatalysts $K_4Ce_2M_{10}O_{30}$ (M = Ta, Nb) for hydrogen evolution from water decomposition

Mengkui Tian[a,b,c], Wenfeng Shangguan[a,*], Jian Yuan[a], Shijie Wang[b], Ziyuan Ouyang[b]

[a]*Research Center for Combustion and Environment Technology, Shanghai Jiao Tong University, Shanghai 200030, PR China*
[b]*State Key Laboratory of Environmental Geochemistry, Geochemistry Institute of Chinese Academy of Sciences, Guiyang, Guizhou, 550002, PR China*
[c]*Graduate School of Chinese Academy of Sciences, Beijing 100047, PR China*

Received 21 July 2006; received in revised form 30 August 2006; accepted 1 September 2006
Available online 20 October 2006

Abstract

Metal oxide photocatalysts $K_4Ce_2M_{10}O_{30}$ (M = Ta, Nb) capable of responding to visible light were synthesized by conventional high temperature solid-state reaction. The photocatalysts have an appropriate band gap energy ca. 1.8–2.3 eV and excellent chemical potential level to evolve H_2 from aqueous solutions containing a sacrificial electron donor (Na_2SO_3) under visible light irradiation ($\lambda > 420$ nm) without any co-catalyst. When they were loading with Pt, RuO_2 and NiO_x, the activities for evolving H_2 were prompted markedly. By SEM and TEM investigations, it can be seen that these loading metal and metal oxides are dispersed on the surface of photocatalysts $K_4Ce_2M_{10}O_{30}$ (M = Ta, Nb) in diameter of about 10–30 nm particles, especially the NiO_x loading even formed double layered structure with metal nickel (Ni) and metal oxide (NiO). The reasons for the increasing activities after these loading may be attributable to facilitate electron migrating from the conduction band of $K_4Ce_2M_{10}O_{30}$ (M = Ta, Nb) to the Pt, RuO_2 and NiO_x nanoparticles, which function as H_2 production sites on the surface of catalysts. The same phenomenon appears on the solid solution $K_4Ce_2Ta_{10-x}Nb_xO_{30}$ ($x = 0-10$) with loading RuO_2.

Keywords: Visible-light driven; Photocatalyst; $K_4Ce_2M_{10}O_{30}$ (M = Ta; Nb); Water decomposition

1. Introduction

The development of H_2 as a renewable energy is well believed to be a potential way to solve the current energy and environmental problems. At present, hydrogen is mainly produced by steam reforming of hydrocarbons such as methane in industry, but from a long and ideal run, it must be produced from water using a renewable energy source such as solar energy when takes the cost and environmental issues into consideration. Using semiconductor photocatalysts to decompose water into H_2 under irradiation is one of the most promising ways to develop H_2 energy. The most important work in photocatalytically decomposing water into H_2 process is to develop semiconductor photocatalysts capable of responding to visible light and possessing high quantum yield. Based on this, series of semiconductor compounds were investigated and different modified ways were intensively studied to prompt their activities. Among these, loading of noble metal or metal oxide such as Pt, RuO_2 and NiO_x to prompt H_2 evolution activities have been intensively practiced [1–7].

In the present paper, metal oxide photocatalysts $K_4Ce_2M_{10}O_{30}$ (M = Ta, Nb) capable of responding to visible light were presented. The photocatalysts have an appropriate band gap energy ca. 1.8–2.3 eV, corresponding to absorption edge of 540–690 nm, and excellent chemical potential level for utilization of solar energy to evolve H_2 from aqueous solutions containing a sacrificial electron donor (Na_2SO_3) under visible light irradiation ($\lambda > 420$ nm) without any co-catalyst. When they were loading with Pt, RuO_2 and NiO_x, the activities of

*Corresponding author. Tel.: +86 21 64076226; fax: +86 21 64075359.
E-mail address: shangguan@sjtu.edu.cn (W. Shangguan).

1468-6996/$ - see front matter © 2006 NIMS and Elsevier Ltd. All rights reserved.
doi:10.1016/j.stam.2006.09.001

evolving H_2 were prompted markedly. The solid solution $K_4Ce_2Ta_{10-x}Nb_xO_{30}$ ($x = 0-10$) showed photocatalytic activities consistent with their photophysical properties and also the remarkable promotion effect with loading RuO_2.

2. Experimental

2.1. Preparation and characterization of materials

$K_4Ce_2M_{10}O_{30}$ (M = Ta, Nb) were synthesized from high purity $K_2CO_3 \cdot 3H_2O$, $Ce(NO_3)_3 \cdot 6H_2O$, Ta_2O_5 (or Nb_2O_5) through conventional high temperature solid-state reactions, first at 800 °C for 5 h then 1100 °C for 12 h, with a regrinding process in between. Excess $K_2CO_3 \cdot 3H_2O$ (ca. 20%) was used to compensate for the loss caused by volatilization during calcination. After the reaction, the product was washed with distilled water and dried. The solid solution compounds of Ta and Nb phases, denoted as $K_4Ce_2Ta_{10-x}Nb_xO_{30}$ ($x = 0-10$), followed the same procedures above with corresponding ratio between Ta_2O_5 and Nb_2O_5.

Pt of 0.3 wt% was in situ photodeposited on the $K_4Ce_2M_{10}O_{30}$ catalysts from precursor of $H_2PtCl_6 \cdot 6H_2O$, and RuO_2 was loaded by impregnation of $RuCl_3 \cdot 3H_2O$ and then calcinated at 500 °C for 2 h in atmosphere, as reported [8]. The 1.0 wt% NiO_x-loaded photocatalysts were obtained through calcination at 350 °C for 1 h in air after drying the mixture of powder samples with aqueous $Ni(NO_3)_2$ solution at 80 °C. As-prepared photocatalysts loaded with NiO were further reduced in H_2 atmosphere at 500 °C for 2 h, then, treated in air atmosphere at 200 °C for 1 h. The samples followed with this reduction–oxidation procedure were denoted as NiO_x loading [6].

The resulting samples were identified by X-ray diffraction on Bruker–AXS D8 Advance with Cu-Kα radiation ($\lambda = 1.540562$ Å). UV–Vis diffuse reflectance spectra were measured using TU-1901 spectrophotometer. The reflectivity spectrum was transformed to absorbance intensity through Kubelka–Munk method. The BET surface areas of the $K_4Ce_2M_{10}O_{30}$ (M = Ta, Nb) powders were determined from N_2 adsorption–desorption isotherm on Quantachrome NOVA 1000-TS. The SEM was recorded on FEI SIRION 200 and TEM on JEM1200EX with accelerating voltage of 80 kV.

2.2. Measurement of photocatalytic activity

The photocatalytic reaction was carried out in a photoreactor, which was provided with an entry window of optical flat quartz glass of ca. 64.0 cm^2. Photocatalyst powder of 0.1 g was dispersed and suspended in 20 mL of aqueous solution in the reactor under the vertical irradiation with 300 W Xe lamp. Visible light irradiation condition was carried out through a glass cut-off filter ($\lambda > 420$ nm) to remove UV light. H_2 and O_2 evolutions were measured by gas chromatography (QC-9101) with thermal conductivity detector (TCD) and high-purity Ar as carrier gas.

3. Results and discussions

3.1. Light absorbance properties and electronic structure of $K_4Ce_2M_{10}O_{30}$ (M = Ta, Nb)

The resulting powders of $K_4Ce_2M_{10}O_{30}$ (M = Ta, Nb) had an X-ray diffraction pattern consistent with the tetragonal tungsten bronze structured [9], being in parallelepiped morphological structure. The UV–Vis diffuse reflectance spectra of $K_4Ce_2M_{10}O_{30}$ (M = Ta, Nb) are shown in Fig. 1. The absorption edge of $K_4Ce_2Ta_{10}O_{30}$ is at about 540 nm, corresponding to band gap energy of 2.3 eV; and the absorption edge of $K_4Ce_2Nb_{10}O_{30}$ is at about 690 nm, corresponding to band gap energy of 1.8 eV. Their absorbance properties are consistent with their appearance colors (golden yellow for $K_4Ce_2Ta_{10}O_{30}$, while $K_4Ce_2Nb_{10}O_{30}$ appeared deep brown). The as-prepared $K_4Ce_2M_{10}O_{30}$ (M = Ta, Nb) catalysts present a band gap energy near 2.0 eV, which is regarded as a very appropriate level for photocatalytic water splitting [2].

It is well known that electronic structure is an important factor dominating materials' properties and the study of it is necessary to bridge their relationship between structure and properties. Quantum mechanical calculations provide a means to understand and to predict the interactions between atoms and molecules and to model chemical reactions on a microscopic scale. Atomistic computational technologies (computational quantum mechanics, molecular simulations and molecular mechanics) are an effective way to bridge the gap between fundamental materials science and materials engineering [10]. First-principle calculation based on density functional theory (DFT) has been extensively used to study the electronic structures of materials. By first-principle calculation based on DFT within general gradient approximation (GGA) and

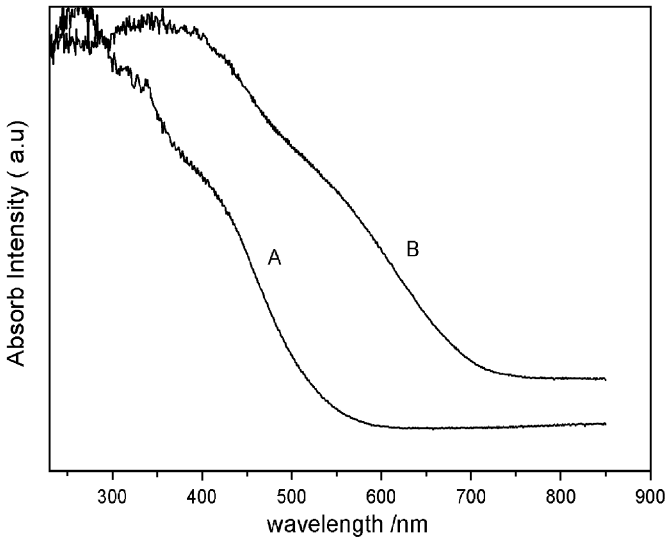

Fig. 1. UV–Vis diffuse reflectance spectra of $K_4Ce_2M_{10}O_{30}$ for (A) M = Ta, and (B) M = Nb.

plane-wave pseudopotential (PWP) method [11], the obvious results obtained firstly are that the band gap of $K_4Ce_2M_{10}O_3$ is 1.6 eV for M = Ta and 1.1 eV for M = Nb. The band gap calculated by DFT was smaller than that obtained experimentally, which is frequently pointed out as a common feature of DFT calculations for the discontinuity in the exchange-correlation potential is not taken into account within the framework of density functional theory [12]. From the close investigations of the band structure and the partial density of states, it can be proposed that their valence bands are composed of hybridization with O2p + Ta5d (or Nb4d) and occupied Ce4f orbitals, the conduction bands of these photocatalysts $K_4Ce_2M_{10}O_{30}$ (M = Ta, Nb) are mainly attributable to the Ta5d (or Nb4d) orbitals. Although the unoccupied Ce4f orbitals have overlap in the bottom of conduction band, they are less effective in transferring electrons and photocatalytic activities for their highly localized nature. The contribution of these orbitals to the energy bands affects the electronic structure of both the photocatalysts and gives rise to their differences in light absorption and photocatalytic activities [13].

3.2. Photocatalytic H_2 evolution on $K_4Ce_2M_{10}O_{30}$ (M = Ta, Nb) loading with Pt, RuO_2 and NiO_x

H_2 evolution on $K_4Ce_2M_{10}O_{30}$ (M = Ta, Nb) without any loading and loading with Pt, RuO_2 and NiO_x in aqueous Na_2SO_3 solution under visible light ($\lambda > 420$ nm) were shown in Fig. 2. As shown in Fig. 2, the activities for H_2 evolution on photocatalysts loading with Pt, RuO_2 and NiO_x were prompted markedly compared with those without any loading. The amount of H_2 evolution in Na_2SO_3 solution under visible light irradiation ($\lambda > 420$ nm) for 4 h on NiO_x-loading $K_4Ce_2M_{10}O_{30}$ reached 135 μmol (M = Ta) and 51 μmol (M = Nb), respectively, which is about 4–7 times of that loading with Pt or RuO_2, and 10–15 times of that without any loading.

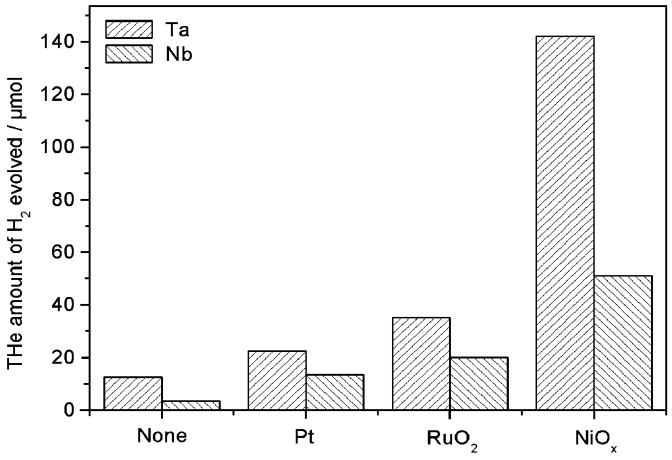

Fig. 2. H_2 evolution of photocatalysts $K_4Ce_2M_{10}O_{30}$ (M = Ta, Nb) without loading and with loading of Pt, RuO_2 and NiO_x, 0.1 g catalyst dispersing in 20 ml 0.2 M Na_2SO_3 solution under visible light irradiation ($\lambda > 420$ nm) for 4 h.

The SEM images of photocatalysts $K_4Ce_2M_{10}O_{30}$ (M = Ta, Nb) without loading, with loading Pt, RuO_2 and NiO_x are shown in Fig. 3. In SEM recording, it can be seen that these loading metal or metal oxide are dispersed on the surface of photocatalysts $K_4Ce_2M_{10}O_{30}$ (M = Ta, Nb) with diameter of 10–30 nm particles. Especially, following the reduction–oxidation procedure denoted as NiO_x loading, it formed the metal Ni and metal oxide NiO double layer structure loading in order, as shown in the TEM images in Fig. 4. The reasons for the increasing activities after these loading may be attributable to the facilitation of electron migration from the conduction band of $K_4Ce_2M_{10}O_{30}$ (M = Ta, Nb) to the Pt, RuO_2 and NiO_x nanoparticles, which function as H_2 production sites on the surface of catalysts [14]. The parallelepiped (tunnel) surface structure of $K_4Ce_2M_{10}O_{30}$ (M = Ta, Nb) is beneficial to the formation of "nest", where nanoparticles of Pt, RuO_2 and NiO_x are strongly associated, improving the photocatalytic activity greatly [15]. Furthermore, since the surface NiO works as a H_2 evolution site, electrons photogenerated in photocatalysts have to cross the interface between photocatalysts and loaded co-catalyst to reach the surface for reducing water. In this case, the barrier for the electron crossing the interface between heat-treated Ni metal and oxide photocatalysts seems to be lower than that at the interface between NiO and oxide photocatalysts. Thus, the double-layered structure of nickel formed by the treatment of reduction–oxidation is easier to assist the electron transfer from photocatalysts to co-catalysts and retention of the back reaction of H_2 and O_2 on surface [16], therefore, this loading showed the highest activities for H_2 evolution compared with other current loadings. It is worth noting that the activities for H_2 evolution on $K_4Ce_2Ta_{10}O_{30}$ are more excellent than that on $K_4Ce_2Nb_{10}O_{30}$ (as seen in Fig. 2), although the band gap of $K_4Ce_2Nb_{10}O_{30}$ (1.8 eV) is narrower than that of $K_4Ce_2Ta_{10}O_{30}$ (2.3 eV) and the BET surface area of M = Ta (1.67 m^2/g) is smaller than that of M = Nb (2.65 m^2/g). From previous study, there is suggestion that the difference in the photocatalytic properties between isostructure tantalates and niobates is mainly due to the difference in their band structure rather than their difference in light absorption and surface properties [13]. It is well known that Ta5d level is higher than that of Nb4d, The higher the level of conduction band edge, the higher reduction ability it possesses, therefore, resulting in the driving force for H_2 evolution on $K_4Ce_2Ta_{10}O_{30}$ is more powerful than that on $K_4Ce_2Nb_{10}O_{30}$, and so do those with loading of Pt, RuO_2 and NiO_x.

In general, the effect for the H_2 evolution on the interaction between these widely used co-catalysts (Pt, RuO_2, NiO_x) and conventional electron donors (Na_2SO_3, CH_3OH) is little taken into consideration. In order to check the effect of these co-catalysts with Na_2SO_3 aqueous solution on H_2 evolution in the absence of as-prepared

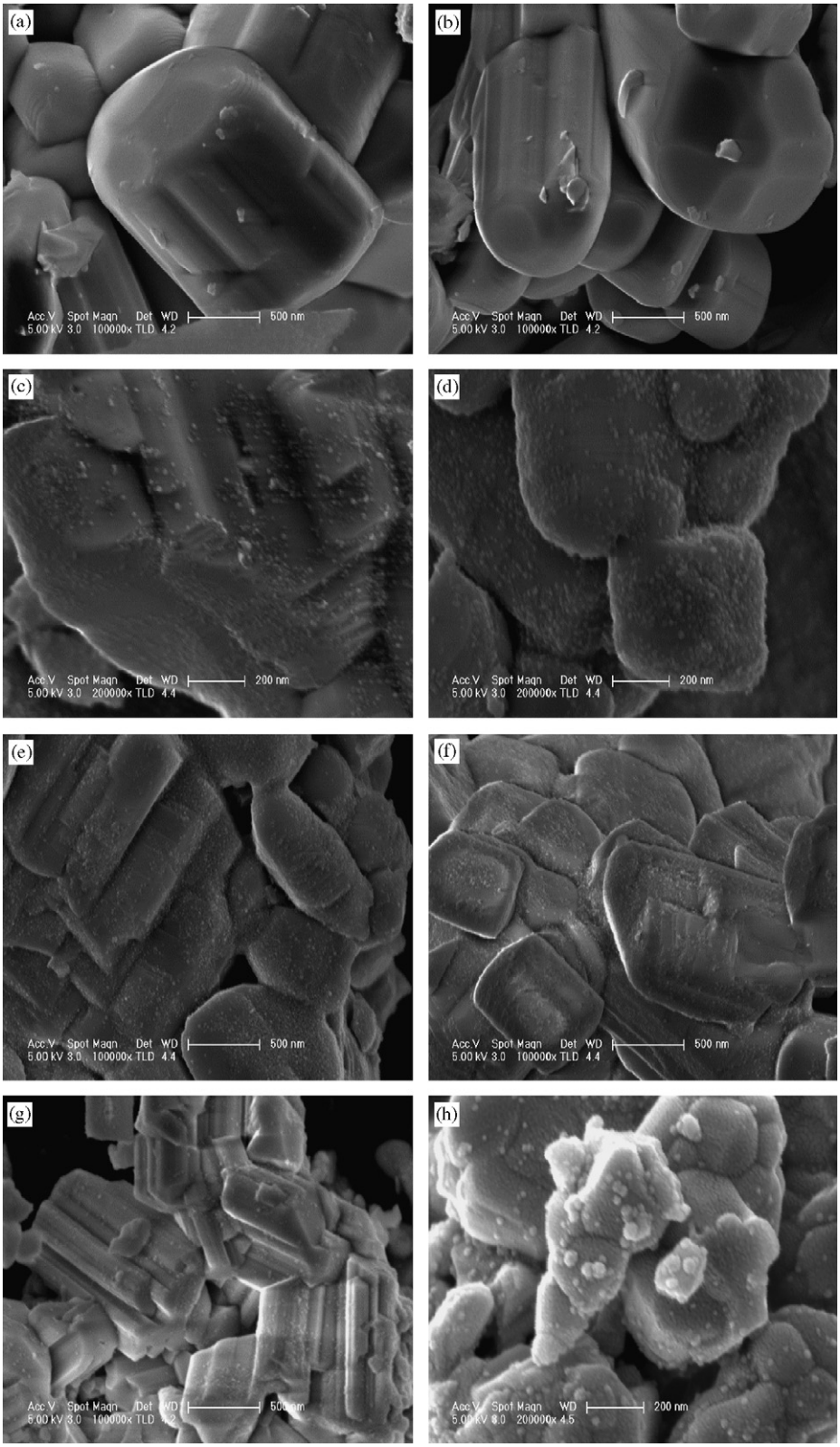

Fig. 3. The SEM micrograph of photocatalysts $K_4Ce_2M_{10}O_{30}$ (M = Ta, Nb) without loading ((a): M = Ta, (b): M = Nb), with loading Pt((c): M = Ta, (d): M = Nb)), RuO_2 ((e): M = Ta, (f): M = Nb)) and NiO_x ((g): M = Ta, (h): M = Nb).

photocatalysts $K_4Ce_2M_{10}O_{30}$ (M = Ta, Nb) under visible light irradiation, Pt (0.3 wt%), RuO_2 (1.0 wt%), and NiO_x (1.0 wt%) were loaded, respectively, by the same procedures on TiO_2 (P25), which is only active under UV light. Photocatalytic reactions were carried out in Na_2SO_3 aqueous solution under the visible light irradiation

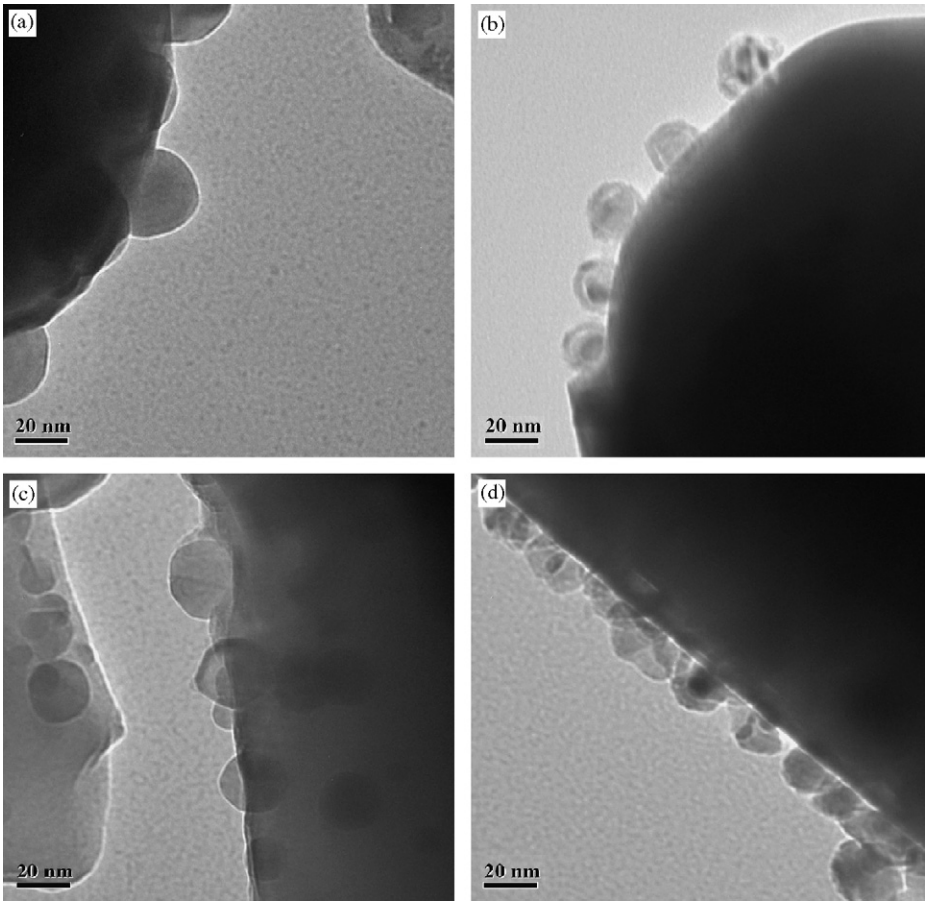

Fig. 4. The TEM images of photocatalysts $K_4Ce_2M_{10}O_{30}$ (M = Ta, Nb) with NiO and NiO_x anchoring on. (a) and (b) represent NiO and NiO_x anchoring on M = Ta phase; while (c) and (d) are for M = Nb phase with NiO and NiO_x anchoring, respectively.

($\lambda > 420$ nm). Hardly any evolved H_2 was examined for long time. Therefore, it can be confirmed that the H_2 evolution on $K_4Ce_2M_{10}O_{30}$ (M = Ta, Nb) loading with Pt, RuO_2, NiO (NiO_x) in Na_2SO_3 solution under visible light irradiation is ascribed to the photocatalytic reaction.

4. Photocatalytic activity of solid solution $K_4Ce_2Ta_{10-x}Nb_xO_{30}$ ($x = 0-10$)

Usually, tantalates and niobates form isostructure compounds for the similar properties of atom Ta and Nb, especially the diameter of their cations (0.68 Å for Ta^{5+} and 0.69 Å for Nb^{5+}). There is no exception in the current system $K_4Ce_2M_{10}O_{30}$ (M = Ta, Nb), being in the same tetragonal tungsten bronze structure. Their solid solution compounds $K_4Ce_2Ta_{10-x}Nb_xO_{30}$, the values of x ranging from 0 to 10, also posed the same tetragonal tungsten bronze [9], as their XRD patterns shown in Fig. 5. The UV–Vis diffuse reflectance spectra of these solid solution compounds are shown in Fig. 6. From the UV–Vis spectra, it is demonstrated that with increased amount of Nb, the absorbance edges shift to red zone, correspondingly, and they show the band transition absorption

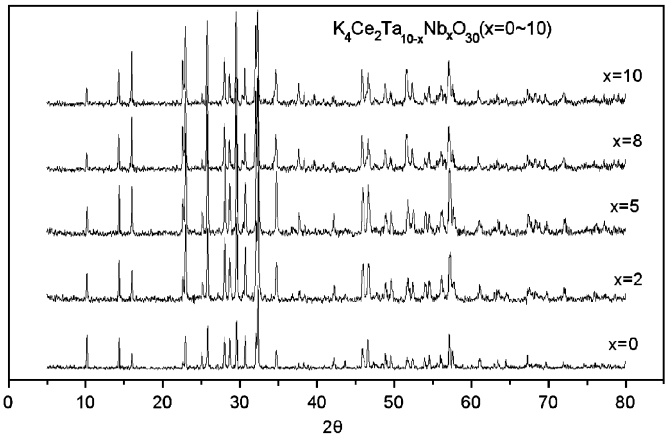

Fig. 5. XRD patterns of $K_4Ce_2Ta_{10-x}Nb_xO_{30}$ ($x = 0-10$).

properties. Furthermore, the UV–Vis spectrum of physical mixture of powder samples of pure Ta and Nb phases is also shown in Fig. 6. The physical mixture displayed obvious two absorption edges belonging to pure phase of M = Ta and M = Nb, respectively, which further confirmed the formation of single phase solid solution

compounds of Ta and Nb through high-temperature solid-state reaction. Their photocatalytic activities for H_2 evolution on without loading and loading with RuO_2 under visible light irradiation in the presence of sacrificial electron acceptor Na_2SO_3 aqueous solution are shown in Fig. 7. On these without any loading, their activities for H_2 evolution decreased with the increase of Nb amount in $K_4Ce_2Ta_{10-x}Nb_xO_{30}$ ($x = 0-10$), and the activities of these solid solution compounds are between these of single-phase Ta and Nb. The reason for this phenomenon may be ascribed to their differences in conduction bands. As the results of the electronic structures analysis shown in our previous work [13], the higher photocatalytic activity of $K_4Ce_2Ta_{10}O_{30}$ than that of $K_4Ce_2Nb_{10}O_{30}$ is due to the higher chemical potential of Ta5d than that of Nb4d, which is proposed to the configuration of their conduction bands, respectively. The higher the conduction band is, the higher the ability to reduce H^+ to H_2 it has. Moreover, the UV–Vis diffuse reflectance spectra of these solid solution compounds indicate their absorbance edges shift to the red region with increased amount of Nb in $K_4Ce_2Ta_{10-x}Nb_xO_{30}$, correspondingly, resulting in the lower band edges and the lower ability to reduce water to H_2, so there showed decreased activities with increased amount of Nb. The same trend appears on those loaded with RuO_2, and the remarkable promotion effect on their photocatalytic activities are also attributed to the electron migration from the conduction band of $K_4Ce_2Ta_{10-x}Nb_xO_{30}$ ($x = 0-10$) to the RuO_2 nanoparticles, which function as H_2 production sites on the surface of catalyst.

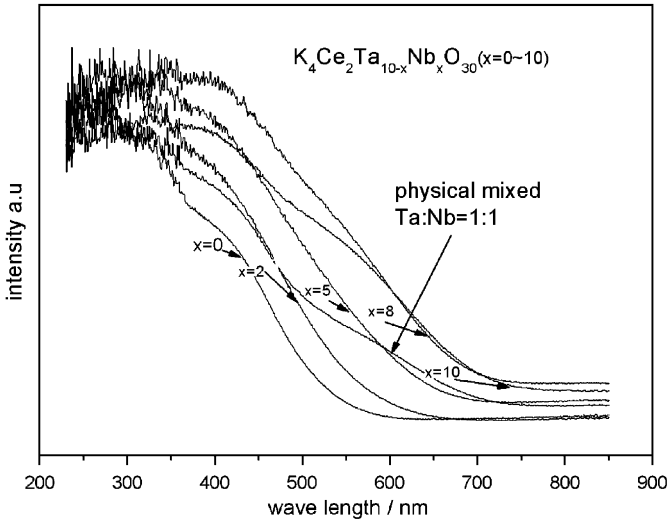

Fig. 6. UV–Vis diffuse reflectance spectra of $K_4Ce_2Ta_{10-x}Nb_xO_{30}$ ($x = 0-10$).

5. Conclusion

Metal oxide photocatalysts $K_4Ce_2M_{10}O_{30}$ (M = Ta, Nb) capable of responding to visible light were presented. The photocatalysts have an appropriate band gap energy ca. 1.8–2.3 eV and excellent chemistry potential level for utilization of solar energy to evolve H_2 from aqueous solutions containing a sacrificial electron donor (Na_2SO_3) under visible light irradiation ($\lambda > 420$ nm) without any co-catalyst. When they were loading with Pt, RuO_2 and NiO_x, which disperse on the surface of the host catalyst with diameter of 10–30 nm particles and function as H_2 production sites, the activities of evolving H_2 were prompted markedly, especially following with partial reduction–oxidation procedures denoted as NiO_x loading. The same remarkable promotion effect appears on solid solution $K_4Ce_2Ta_{10-x}Nb_xO_{30}$ ($x = 0-10$) with RuO_2 loading. It can be concluded that loading with noble metal or metal oxide such as Pt, RuO_2 and NiO_x etc. is an efficient way to prompt photocatalytic activities.

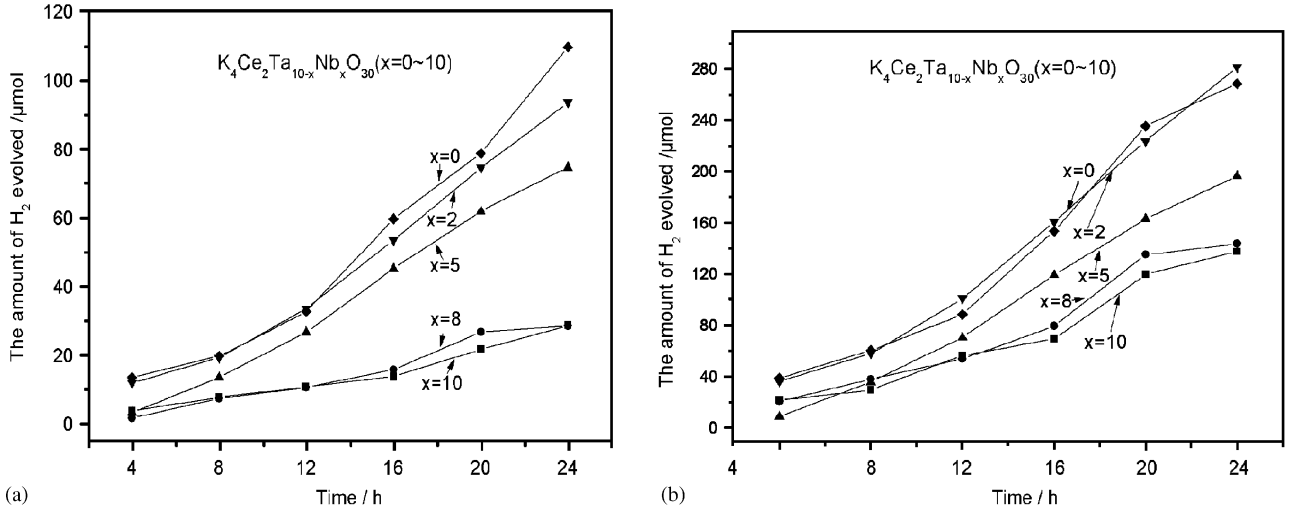

Fig. 7. The activities for H_2 evolution on $K_4Ce_2Ta_{10-x}Nb_xO_{30}$ ($x = 0-10$) without loading (a) and with loading 1 wt% RuO_2, (b) 0.2 g catalyst dispersing in 100 ml 0.2 M Na_2SO_3 solution under visible light irradiation ($\lambda > 420$ nm).

Acknowledgments

This work was financially supported by the National Natural Science Foundation of China (Grant no. 50076026), the National Key Basic Research and Development Program (Grant no. 2003CB214500), and the Trans-Century Training Program Foundation for Talents from the Chinese Ministry of Education.

References

[1] I. Tsuji, H. Kato, H. Kobayashi A. Kudo, J. Am. Chem. Soc. 126 (41) (2004) 13406–13413.
[2] A. Kudo, H. Kato I. Tsuji, Chem. Lett. 33 (12) (2004) 1534–1539.
[3] J. Sato, N. Saito, Y. Yamada, K. Maeda, T. Takata, J.N. Kondo, M. Hara, H. Kobayashi, K. Domen Y. Inoue, J. Am. Chem. Soc. 127 (12) (2005) 4150–4151.
[4] K. Maeda, K. Teramura, D. Lu, T. Takata, N. Saito, Y. Inoue, K. Domen, Nature 440 (2006) 295.
[5] M. Hara, J. Nunoshige, T. Takata, J.N. Kondo K. Domen, Chem. Commun. 24 (2003) 3000–3001.
[6] Z. Zou, J. Ye, H. Arakawa, K. Sayama, Nature 414 (2001) 625–627.
[7] H. Kato, K. Asakura A. Kudo, J. Am. Chem. Soc. 125 (10) (2003) 3082–3089.
[8] W.F. Shangguan, A. Yoshida, J Phys. Chem. B 106 (47) (2002) 12227–12230.
[9] F. Brik, R. Enjalbert, C. Roucau J. Galy, J. Solid State Chem. 122 (1996) 7–14.
[10] J. Hafner, Acta. Mater. 48 (2000) 71–92.
[11] M.D. Sgall, P.J.D. Lindan, M.J. Probert, C.J. Pickard, P.J. Hasnip, S.J. Clark, M.C. Payer, J. Phys.:Condens. Matter 14 (2002) 2717–2744.
[12] J. Sato, N. Saito, Y. Yamada, K. Maeda, T. Takata, J.N. Kondo, M. Hara, H. Kobayashi, K. DomenY. Inoue, J. Am. Chem. Soc. 127 (2005) 4150–4151.
[13] M.K. Tian, W.F. Shangguan, J. Yuan, L. Jiang, M.X. Chen, J.W. Shi, Z.Y. Ouyang, S.J. Wang, Appl. Catal. A 309 (2006) 76–84.
[14] A. Kudo, Int. J. Hydrogen Energy 31 (2006) 197–202.
[15] W.F. Shanguan, A. Yoshida, Int. J. Hydrogen Energy 24 (1999) 425–431.
[16] A. Kudo, H. Kato, S. Nakagawa, J. Phys. Chem. B 104 (3) (2000) 571–575.